Developmental Cell, Vol. 9, 133–145, July, 2005, Copyright ©2005 by Elsevier Inc. DOI 10.1016/j.devcel.2005.05.002

Inositol Polyphosphates Regulate Zebrafish Left-Right Asymmetry

Bhaskarjyoti Sarmah,[1,3] Andrew J. Latimer,[2,3] Bruce Appel,[2,*] and Susan R. Wente[1,*]
[1]Department of Cell and Developmental Biology
Vanderbilt University Medical Center
U-3209 MRBIII
465 21st Avenue South
Nashville, Tennessee 37232
[2]Department of Biological Sciences
Vanderbilt University
2401 Stevenson Center
1161 21st Avenue South
Box 35-1634
Nashville, Tennessee 37232

Summary

Vertebrate body plans have a conserved left-right (LR) asymmetry manifested in the position and anatomy of the heart, visceral organs, and brain. Recent studies have suggested that LR asymmetry is established by asymmetric Ca^{2+} signaling resulting from cilia-driven flow of extracellular fluid across the node. We report here that inositol 1,3,4,5,6-pentakisphosphate 2-kinase (Ipk1), which generates inositol hexakisphosphate, is critical for normal LR axis determination in zebrafish. Zebrafish embryos express *ipk1* symmetrically during gastrulation and early segmentation. *ipk1* knockdown by antisense morpholino oligonucleotide injection randomized LR-specific gene expression and organ placement, effects that were associated with reduced intracellular Ca^{2+} flux in cells surrounding the ciliated Kupffer's vesicle, a structure analogous to the mouse node. Our data suggest that the pathway for inositol hexakisphosphate production is a key regulator of asymmetric Ca^{2+} flux during LR specification.

Introduction

Inositol signaling pathways directly regulate cell proliferation, differentiation, and apoptosis (Berridge et al., 2000; Irvine, 2003). The effects are initiated by extracellular stimuli inducing changes in lipid and soluble inositol polyphosphates (IPs) levels, resulting in essential second messengers that amplify and propagate signals to intracellular targets. For soluble inositides, lipid-anchored phosphatidylinositol 4,5-bisphosphate (PIP_2) is the effective starting point with regulated hydrolysis by phospholipase C (PLC) producing diacylglycerol (DAG) and soluble inositol 1,4,5-triphosphate (IP_3) (Irvine, 2003). IP_3 regulates the release of intracellular Ca^{2+}, whereas DAG activates protein kinase C (Berridge et al., 2000). IP_3 is also the substrate for generation of all other soluble IPs. For example, IP_3 is sequentially phosphorylated to produce inositol tetrakisphosphate (IP_4) isomers, inositol 1,3,4,5,6-pentakisphosphate (IP_5), inositol hexakisphosphate (IP_6), and inositol pyrophosphates (e.g., IP_7) (Irvine and Schell, 2001; Odom et al., 2000; Shears, 2004; York et al., 1999). Each isomer is potentially generated by coordinated actions of specific kinases and phosphatases.

Perturbations of inositol signaling result in pathophysiological states that include cancer of the brain, prostate, and skin and neurological disorders (Pendaries et al., 2003). However, the normal cellular functions for many of these IPs are unknown. Previous work has shown that the yeast *S. cerevisiae* IP_3 to IP_6 pathway regulates vital cellular processes such as nuclear mRNA export, chromatin remodeling, and transcription (Odom et al., 2000; Shen et al., 2003; Steger et al., 2003; York et al., 1999). Studies using mammalian cells have linked IP_6 to roles as diverse as the regulation of Ca^{2+} channels, nonhomologous end joining in DNA repair, mRNA export, endocytosis, and exocytosis (Irvine and Schell, 2001; Shears, 2004). The role of IP_6 production in vertebrate disease or development has not been reported.

In vertebrate development, the precise regulation of cell signaling events is essential. Ca^{2+} signaling has been linked to several developmental processes (Webb and Miller, 2003), including establishment of the left-right (LR) asymmetry fundamental to vertebrate body plans (McGrath et al., 2003; Webb and Miller, 2003). Early embryogenesis involves a major transformation from a radially symmetric blastoderm into a bilaterally symmetric embryo within which LR asymmetry is subsequently established with induction of LR-specific gene expression and later LR morphogenesis of the heart, visceral organs, and brain (Capdevila et al., 2000; Wright, 2001). Laterality defects that arise from failure to establish LR asymmetry fall into two groups: those that do not break bilateral symmetry (isomerisms) and those unable to orient LR asymmetry properly, causing either inversion of LR anatomy (situs inversus) or discordant LR morphogenesis (most often referred to as heterotaxia) (Capdevila et al., 2000).

Studies in mice have suggested that a leftward extracellular flow (termed nodal flow) across the surface of the embryonic node, generated by dynein-dependent rotation of motile monocilia, might break LR symmetry (Nonaka et al., 1998; Nonaka et al., 2002; Okada et al., 1999). In one model, this flow causes the advection of a morphogen to an asymmetric distribution, which then initiates downstream molecular and morphogenetic events (reviewed in Tabin and Vogan, 2003). Another model involves nonmotile cilia, which contain the cation channel polycystin-2, acting as mechanosensors of nodal flow. Nodal flow-induced flexing causes an asymmetric Ca^{2+} flux at the left border of the node and subsequent asymmetric gene expression (McGrath et al., 2003). Structures similar to the node, with monociliated cells, are found in other vertebrate embryos, including Kupffer's vesicle (KV) in zebrafish (Cooper and D'Amico, 1996; Essner et al., 2002). Evidence that LR

*Correspondence: b.appel@vanderbilt.edu (B.A.); susan.wente@vanderbilt.edu (S.R.W.)
[3]These authors contributed equally to this work.

asymmetry may also be influenced by extracellular Ca^{2+} in the chicken embryo was recently reported (Raya et al., 2004). However, it is not clear if these two proposed roles for Ca^{2+} are linked. Other studies have raised the possibility that gap junctions, H^+/K^+ ATPase, and PKC-γ function in specification of LR asymmetry in frogs and that H^+/K^+ ATPase activity is also important for chick LR asymmetry (Kramer et al., 2002; Levin and Mercola, 1998; Levin et al., 2002). Whether these various factors play conserved or distinct roles in the initial breaking of symmetry or for maintenance and propagation of LR asymmetry in different vertebrate species is not known. Nevertheless, all vertebrates that have been investigated exhibit asymmetric expression of homologous genes. For example, left lateral plate mesoderm (LPM) expresses intercellular signaling molecules such as *nodal*, *lefty1*, and *lefty2*, and the homeobox transcription factor gene *pitx2* (Hamada et al., 2002). Our current understanding of the mechanisms that promote asymmetric gene expression as a consequence of LR symmetry-breaking events in any vertebrate species is poor.

Here we show that the enzyme Ipk1, an IP_5 2-kinase responsible for IP_6 production, is required for zebrafish LR gene expression and morphogenesis. This documents a role of inositol signaling in LR asymmetry establishment and shows a requirement for the pathway linked to IP_6 production in a crucial aspect of the vertebrate development. Moreover, we connect proper IP_6 production to the generation of intracellular Ca^{2+} flux in cells surrounding KV. We propose that IPs mediate amplification and propagation of the Ca^{2+} signal initiated by a conserved ciliary-based mechanism to multicellular fields.

Results

Symmetric Expression of Zebrafish *ipk1,* Encoding an IP_5 2-Kinase, during Embryogenesis

We identified zebrafish *ipk1* by searching the zebrafish EST database (NCBI). All four highly conserved regions of human (hs) and yeast *S. cerevisiae* (sc) Ipk1 were represented in the zebrafish ESTs. Compilation revealed a 1452 base pair ORF with a predicted protein 57% identical to hsIpk1 (Figure 1A). Searching zebrafish genome database (Ensembl, Sanger Institute) identified the genomic region for the ORF in a 22 kb span interrupted by 12 introns (see Supplemental Figure S1 available with this article online). PCR amplification confirmed that the composite sequence represented a single gene (Supplemental Figure S1). Expression of zebrafish *ipk1* complemented the synthetic lethal phenotype of yeast *gle1-2 ipk1-4* mutant cells (Figure 1B; York et al., 1999) and restored IP_6 production in a *sc-ipk1* null strain (Figure 1C), similar to *hsIPK1* (Verbsky et al., 2002). We conclude that zebrafish *ipk1* encodes a functional IP_5 2-kinase.

We examined zebrafish *ipk1* expression during development using RNA in situ hybridization. *ipk1* RNA was present in cleavage-stage embryos (Figure 2A), indicating maternal deposition, and was ubiquitously distributed throughout blastula stages of embryogenesis (Figure 2B). At the onset of gastrulation, *ipk1* expression appeared enriched in cells around the blastoderm margin (Figure 2C). At shield stage, expression was detected in the deep involuted cells that contribute to mesendoderm (Figures 2D–2F). During mid and late gastrula stages, axial mesendoderm expressed *ipk1* strongly (Figures 2G–2I). However, it was not present in the nascent tailbud at yolk plug closure (YPC) stage (Figure 2H). Expression in axial mesendoderm was reduced at the 2 somite stage (SS) (Figure 2J). At 6 SS, cells surrounding, but apparently not within, KV expressed *ipk1* (Figures 2K and 2L). By 10 SS, *ipk1* RNA was no longer detected as a specific signal above background (data not shown).

KV arises from dorsal forerunner cells (DFCs), which migrate ahead of involuting dorsal blastoderm during gastrulation and express *ntl* (Amack and Yost, 2004; Cooper and D'Amico, 1996). We directly compared *ipk1* and *ntl* expression in DFCs (Figures 2M–2O). Cells at the blastoderm margin express both *ipk1* (Figure 2M) and *ntl* (Figure 2N) at shield stage, and *ntl* is also present in DFCs (arrowhead, Figures 2N and 2O). However, no *ipk1* RNA was evident in definitive DFCs (arrowhead, Figures 2N and 2O).

ipk1 Knockdown Alters IP Levels and Randomizes Heart Asymmetry

We performed *ipk1* loss-of-function experiments by injecting cleavage-stage embryos with an antisense morpholino oligonucleotide (*ipk1*^{MO1} embryos) designed to block translation of *ipk1* mRNA (Supplemental Figure S2). To test the metabolic effects on IP production, the embryos were coinjected with ^{3}H-inositol and harvested at 11.5 hr postfertilization (hpf). The soluble IPs were extracted and analyzed by HPLC (Figure 3J). Wild-type embryos showed a peak of IP_3 with minimal levels of other IPs. In contrast, *ipk1*^{MO1} embryos had marked increases in IP_4 and IP_5. Increased IP_5 is a robust indicator of inhibited IP_6 production in yeast and *Drosophila* cells (Figure 1C; Ives et al., 2000; Seeds et al., 2004; York et al., 1999). Thus, the *ipk1*^{MO1} effectively perturbed *ipk1* function and the pathway for IP_6 production.

At 28 hpf, *ipk1*^{MO1} embryos appeared morphologically normal except for slightly downwardly curved tails. However, closer examination revealed randomization of heart laterality (Figures 3A–3I). In a population (n = 100) of embryos injected with 7.5 ng *ipk1*^{MO1}, 48% had the heart tube on the left side (normal), whereas 44% had it on the right side (Figure 3I). Embryos with the heart tube on the left developed normal rightward looping (D looping), while those with the heart tube on the right developed leftward looping with the ventricle posterior and left of the atrium (Figures 3A–3H). Only 2% of embryos injected with a 5 nucleotide mismatch control MO had the heart tube positioned on the right (Figure 3I). No other morphological defects were noted through 72 hpf. A similar heart laterality effect was caused by injection of an *ipk1*-specific antisense peptide nucleic acid designed to block translation (*ipk1*^{GripNA}) (Figure 3I). An antisense MO designed to block *ipk1* pre-mRNA splicing (*ipk1*^{MO2}) (Supplemental Figure S2) also perturbed heart laterality. However, the *ipk1*^{MO2} was not as strong as the *ipk1*^{MO1} (at 12.5 ng *ipk1*^{MO2}, 79% with the heart

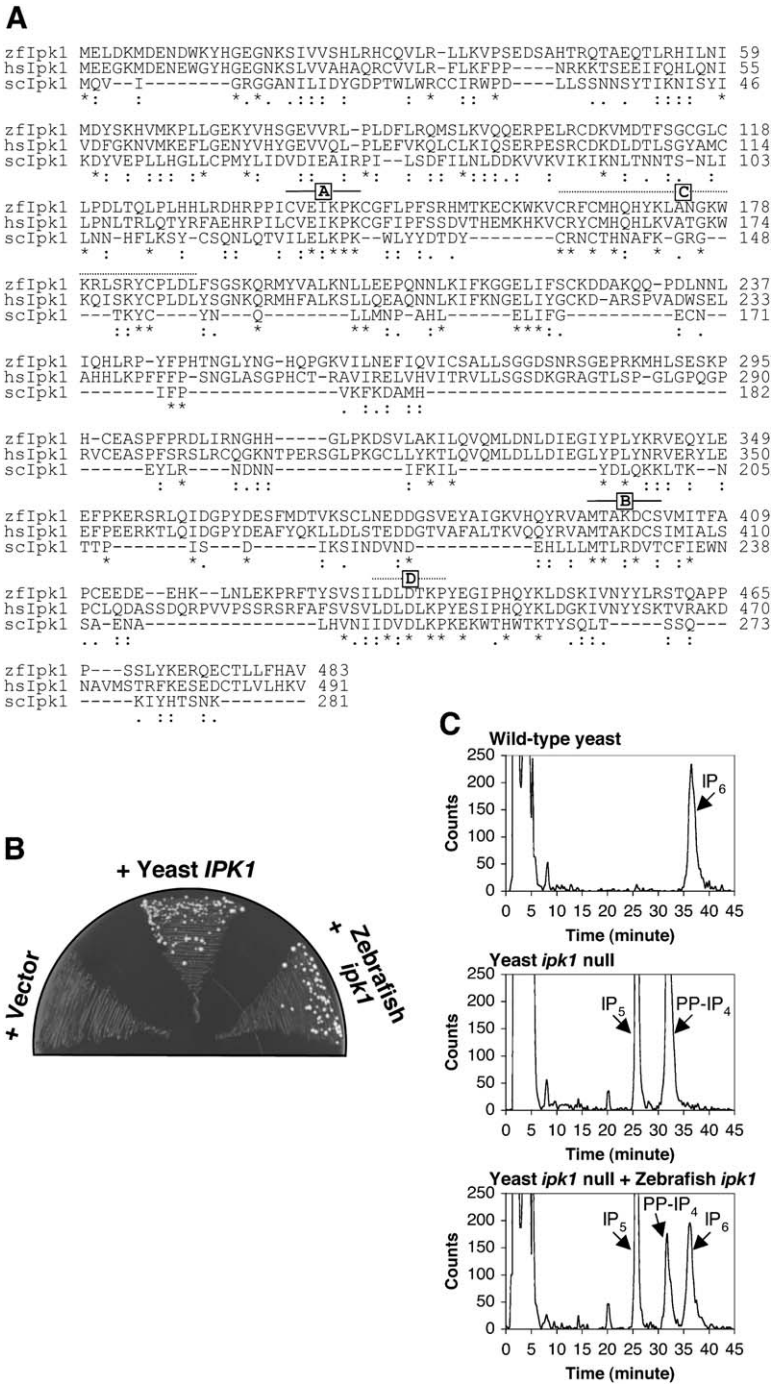

Figure 1. Zebrafish Ipk1 Is a Functional Homolog of Yeast *S. cerevisiae* Ipk1

(A) Sequence alignment of zebrafish (zfIpk1), human (hsIpk1), and yeast *S. cerevisiae* (scIpk1) IP_5 2-kinases (Ipk1) using ClustalW program (Thompson et al., 1994). Identical residues (*), conserved (:), and semiconserved (.) substitutions are marked, and highly conserved regions highlighted (lined A, B, C, D). The sequence data are available from GenBank under accession number DQ075212.

(B) Zebrafish *ipk1* expression complements the synthetic lethal phenotype of the *S. cerevisiae gle1-2 ipk1-4* mutant. Growth for strains SWY2227, SWY2233, and SWY2663 was tested on media containing 5-fluoroorotic acid (5-FOA), and colony formation after 4 days at 23°C is shown.

(C) Zebrafish *ipk1* rescues IP_6 production in a yeast *ipk1* null strain. Wild-type (W303a) (top), *ipk1::KAN*^{r} null mutant (SWY2665) (middle), or the *ipk1::KAN*^{r}-expressing zebrafish *ipk1* (SWY2666) (bottom) yeast strains were grown in complete minimal medium containing [^{3}H] inositol. Soluble IPs were extracted and separated by Partisphere strong-anion exchange HPLC. Labels indicate IP elution positions.

tube leftward and 20% rightward), possibly due to the presence of spliced maternal mRNA. The coinjection of *ipk1*^{MO1} and *ipk1*^{MO2} was synergistic (Figure 3I). At the most effective concentrations for fully randomized left-right placement, a small fraction of the *ipk1*^{MO} or *ipk1*^{GripNA} embryos (5.5% to 9.5%) had an unbent heart tube symmetrically positioned in the midline.

We next examined *bmp4* expression, which at 22 SS is predominantly expressed in the left side of the heart field (Chen et al., 1997). 46% of *ipk1*^{MO1} embryos (n = 65) expressed *bmp4* more highly on the left (normal) versus 42% on the right. The remaining 12% embryos had bilateral expression (Figures 4A and 4H). We attempted rescue experiments by coinjecting either *ipk1* mRNA or an altered *ipk1* mRNA not recognized by the *ipk1*^{MO1}. However, injection of *ipk1* mRNA alone caused perturbations (unpublished data), likely related to unregulated Ipk1 expression that will require future analysis. Overall, the coincident defects in IP levels and heart laterality, preceded by defects in asymmetric gene expression in the heart field, with no other observable developmental perturbations produced by three

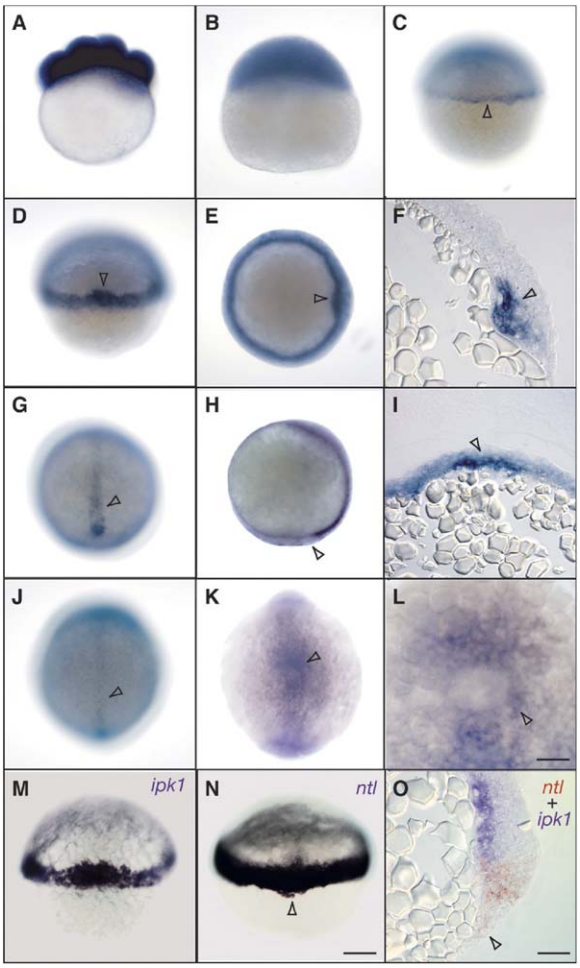

Figure 2. Expression of *ipk1* during Early Zebrafish Embryo Development

RNA in situ hybridizations of whole (A–E, G, H, J–N) or sectioned (F, I, O) embryos.
(A) 8-cell stage embryo showing maternally expressed *ipk1* mRNA.
(B) Lateral view of blastula stage (4 hpf) embryo.
(C) Lateral view of embryo at onset of gastrulation (5 hpf), showing *ipk1* expression in blastoderm margin cells (arrowhead).
(D–F) Shield stage (6 hpf).
(D and E) Dorsal (D) and animal pole (E) views showing *ipk1* expression in cells around the margin of the blastoderm and in the shield (arrowhead).
(F) Sagittal section showing *ipk1* expression in deep cells of the shield (arrowhead).
(G–I) YPC stage (late gastrulation, 10 hpf).
(G) Dorsal view showing *ipk1* expression in axial cells (arrowhead).
(H) Lateral view showing that tailbud cells do not express *ipk1* (arrowhead).
(I) Transverse section through the midline showing that axial hypoblast cells express *ipk1* (arrowhead).
(J) Dorsal view showing reduced axial expression at 2 SS (arrowhead).
(K and L) Ventral views showing *ipk1* expression in cells enveloping KV at 6 SS (arrowhead).
(M and N) Dorsal views of *ipk1* and *ntl* expression, respectively.
(O) Sagittal section showing double-labeled *ntl* and *ipk1* expression in margin cells and shield. Only *ntl* expression is clearly detected in the DFCs (arrowhead, N and O). Scale bar equals 80 μm for (A)–(E), (G), (H), (J), (K), (M), and (N) and 20 μm for (F), (I), (L), and (O).

different loss-of-function reagents, indicated a specific effect.

ipk1 Is Essential for Establishment of Normal Visceral and Diencephalic Asymmetry

We used in situ RNA hybridization to assess whether asymmetry defects in the heart that were caused by *ipk1* knockdown represented a global effect on the asymmetric positioning of visceral organs. LR positioning of the developing gut, revealed by *gata6* (Reiter et al., 1999), was clearly randomized in *ipk1*^{MO1} embryos (7.5 ng/embryo), with 47% left sided and 45% right (Figures 4B and 4H). The heart also expresses *gata6*, and this showed that in all embryos the heart and gut were located either on the same side or both at the midline. LR asymmetry of pancreas and liver (both expressing *foxA3* [Field et al., 2003]) was also randomized in *ipk1*^{MO1}-injected embryos but not affected in control MO-injected embryos (Figures 4C and 4H).

Brain asymmetry was assessed by expression of *lefty1* (Thisse and Thisse, 1999), which is normally expressed on the left side of the diencephalon at 22–24 SS. As with the visceral organs and heart, *ipk1*^{MO1} injection caused randomization of *lefty1* expression in the diencephalon (Figures 4D and 4H). LPM also expresses low levels of *lefty1*, normally on the left side. In most cases, *ipk1*^{MO1} embryos displayed concordant alterations in *lefty1* expression in brain and LPM. LPM did not express *lefty1* on either side in embryos with bilaterally symmetric *lefty1* expression in the brain. Confirmation that asymmetries in the heart and diencephalon were concordant was obtained by double labeling for *bmp4* and *lefty1*. Of 60 *ipk1*^{MO1} embryos, 44% expressed both *lefty1* and *bmp4* on the left, and 41% expressed both genes on the right (Figures 4E and 4H). There were no embryos with *lefty1* and *bmp4* both bilateral. However, 8% expressed *lefty1* bilaterally with *bmp4* either on the left (5%) or right (3%), and 8% did not detectably express *lefty1* but expressed *bmp4* bilaterally (Figure 4E).

The *pitx2*- and *nodal*-related genes show conserved unilateral expression in the left LPM during late somite stages well before asymmetric organ morphogenesis (Essner et al., 2000; Hamada et al., 2002; Rebagliati et al., 1998; Sampath et al., 1998). The normally left-sided expression of *pitx2* (Essner et al., 2000) and the *nodal*-related gene *southpaw* (Long et al., 2003) were randomized in *ipk1*^{MO1}-injected embryos (Figures 4F and 4G, respectively, and Figure 4H). However, laterality defects in *ipk1*^{MO1} embryos did not result from a general failure of LPM development. Bilateral expression of *bmp4* at 18–20 SS indicated that the LPM developed normally in MO-injected embryos (data not shown).

ipk1 Knockdown Perturbs Early Asymmetric Expression of the Nodal-Related Gene *southpaw*

To understand how Ipk1 activity functions in the molecular hierarchy of LR morphogenesis, *ipk1*^{MO1} embryos were examined for the early expression patterns of four genes with roles in LR determination and expression that overlaps temporally with *ipk1*. At 85% epibody, *ntl* is expressed in midline precursor cells, blastoderm margin cells, and DFCs (Schulte-Merker et al., 1994).

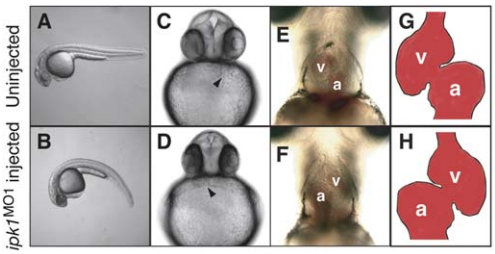

I

Injection	Amount (ng)	N	Heart tube left (%)	Heart tube right (%)	Heart tube midline (%)
Uninjected		93	100		
ipk1^{MO1}	3.75	82	85.4	12.2	2.4
ipk1^{MO1}	5.0	80	67.5	20.0	12.5
ipk1^{MO1}	7.5	100	48.0	44.0	8.0
Control MO	7.5	104	97.1	1.9	1.0
ipk1^{MO2}	5.0	78	92.3	7.7	
ipk1^{MO2}	10.0	80	85.0	13.7	1.3
ipk1^{MO2}	12.5	56	78.6	19.6	1.8
ipk1^{MO1} + *ipk1*^{MO2}	3.75 + 5.0	55	58.2	36.4	5.5
ipk1^{GripNA}	2.5	88	72.7	18.2	9.1
ipk1^{GripNA}	5.0	116	50.0	40.5	9.5

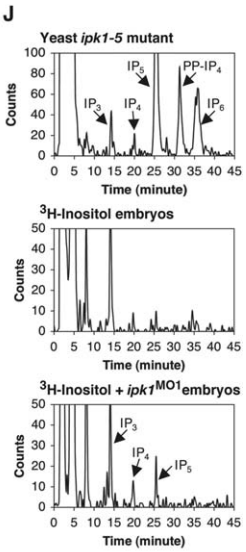

Figure 3. Normal Asymmetry of Heart Tube Placement Is Randomized in *ipk1*-Deficient Embryos

(A and B) Lateral views of live 28 hpf wild-type (A) and *ipk1*^{MO1} (B) embryos.

(C and D) Ventral views of live 28 hpf wild-type (C) and *ipk1*^{MO1} (D) embryos. The heart tube normally jogs left of the midline (C, arrowhead), whereas in *ipk1*^{MO1} embryos, it jogged right (D, arrowhead), left (not shown), or remained on the midline (not shown).

(E and F) Ventral views of 60 hpf wild-type (E) and *ipk1*^{MO1} embryos (F). After jogging left in wild-type embryos, the heart tube loops to the right (E). In *ipk1*^{MO1} embryos, when the heart tube jogged abnormally right, the heart tube looped left (F) (leftward heart tube jogging always resulted in rightward looping, not shown).

(G and H) Schematic diagram demonstrating heart looping in wild-type embryos (G) and *ipk1*^{MO1} embryos with reversed heart looping (H). a, atrium; v, ventricle.

(I) Scores showing effect of *ipk1* loss of function on heart laterality.

(J) *ipk1*^{MO1} injection abolished IP$_6$ production and elevated levels of upstream IPs in zebrafish embryos. Bottom two panels: HPLC profiles of soluble IPs from 4 to 6 SS (11.5 hpf) embryos after injection with ^{3}H-Inositol alone (middle) or with *ipk1*^{MO1} (bottom). Top panel: HPLC profile of an *ipk1-5* mutant yeast strain confirms IP elution positions.

As a T box transcription factor, Ntl functions cell autonomously in DFCs to regulate KV morphogenesis and LR determination (Amack and Yost, 2004). *lefty1* is expressed in midline precursor and margin cells and may act as a midline barrier to signals that determine leftness (Thisse and Thisse, 1999). The *pitx2* gene is expressed in prechordal plate cells during late gastrulation and may function in situs-specific morphogenesis at later stages (Essner et al., 2000). We found that the early expression patterns of *ntl*, *lefty1*, and *pitx2* in *ipk1*^{MO1} embryos were similar to uninjected embryos (Figure 5A).

Previous studies have shown that heart and visceral asymmetries are dependent on normal midline development, and the midline may serve as a boundary to maintain left and right domains (Bisgrove et al., 2000). Midline tissues, including notochord, floor plate, and hypochord, developed normally in *ipk1*^{MO1} embryos (Supplemental Figure S3). This suggests that the downwardly curved tail phenotype in *ipk1*^{MO} embryos is unrelated to midline development. Moreover, this indicates that the role of *ipk1* in LR asymmetry is independent of midline development.

We also examined *southpaw*, the earliest asymmetrically expressed molecular marker in zebrafish (Long et al., 2003). During 4–6 SS, *southpaw* is expressed bilaterally in paraxial mesoderm precursors flanking the tailbud, and expression continues until late stages of somitogenesis. Expression of *southpaw* then becomes asymmetric during 13–15 SS, when it is expressed in the left LPM preceding asymmetric *lefty1* or *pitx2* expression (Long et al., 2003). Although *ipk1*^{MO1} injection did not alter *southpaw* expression in paraxial mesoderm precursors (Figure 5A), expression in the left LPM was perturbed in 13–15 SS embryos, consistent with the disruption of asymmetric expression we observed at 22 SS (Figure 5B). In *ipk1*^{MO1} embryos, the incidence of bilateral *southpaw* expression decreased during late somitogenesis, and expression in the LPM was randomized (Figures 5B and 5C). We conclude that *ipk1* knockdown perturbs early asymmetric expression of *southpaw* and that *ipk1* may function upstream of *southpaw* during establishment of LR asymmetry.

ipk1 Knockdown Does Not Affect KV Morphogenesis

In zebrafish, KV morphogenesis and precise organization and function of ciliated cells are essential for normal LR asymmetry (Amack and Yost, 2004; Essner et al., 2005). Because the cells that surround KV express *ipk1* (Figures 2K and 2L), we compared the morphology of KV and cilia organization in *ipk1*^{MO1}-injected and control embryos (Figures 5D–5G). No differences were detected, indicating that loss of *ipk1* function does not affect KV morphogenesis. This raises the possibility that *ipk1* function is required subsequent to, or coincident with, the role of ciliated KV cells in specifying LR asymmetry but before establishment of LR asymmetric gene expression.

Intracellular Ca^{2+} Fluctuates in Cells Surrounding KV

In mice, the first observed molecular LR asymmetry is elevated intracellular Ca^{2+} flux on the left side of the node (McGrath et al., 2003). Although node monocilia may play key roles in initiating the Ca^{2+} flux, the signaling pathways for propagating this information across cellular fields are unknown. Ipk1 is inherently linked to Ca^{2+} signaling, being downstream of PLC activity and IP$_3$-sensitive Ca^{2+} channels (Berridge et al., 2000; Irvine, 2003). Previous studies have also implicated IP$_4$ and IP$_6$ as regulators of Ca^{2+} channel activity (Hermosura et al., 2000; Larsson et al., 1997; Yang et al., 2001), and in plant guard cells, IP$_6$ serves as a Ca^{2+} release

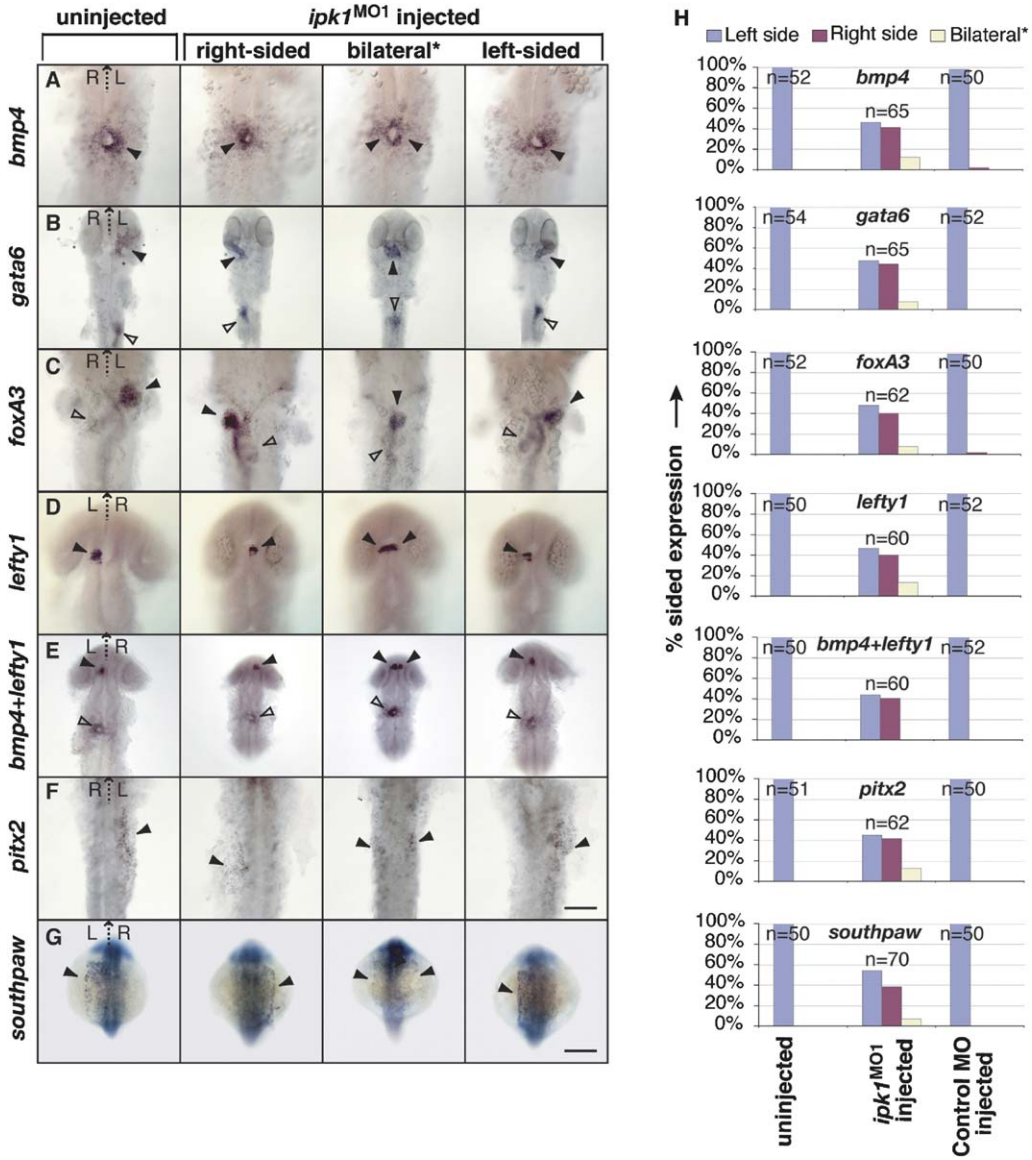

Figure 4. Translational Silencing of *ipk1* Results in Randomized Organ Laterality and LR Gene Expression

(A–G) Whole-mount in situ hybridizations are shown for uninjected (left) and *ipk1*^{MO1} embryos. *Bilateral column designates expression for *bmp4, lefty1, pitx2*, and *southpaw*; midline organ placement for *gata6* and *foxA3*.

(A) Ventral view, 22 SS embryos, showing *bmp4* expression in the heart field (single arrowheads for asymmetric side, double for bilateral).

(B) Ventral view, 30 hpf, showing *gata6* at the heart (filled arrowhead) and gut (open arrowhead).

(C) Ventral view, 48 hpf, showing *foxA3* at the liver (filled arrowhead) and pancreas (open arrowhead).

(D) Dorsal view, 22–24 SS, showing asymmetric or bilateral *lefty1* in the diencephalon (single arrowheads for asymmetric side, double for bilateral).

(E) Dorsal view, 22–24 SS, showing *lefty1* in the diencephalon (filled arrowhead) and *bmp4* in the heart field (open arrowhead).

(F) Ventral view, 22 SS, showing *pitx2* in the LPM (arrowhead).

(G) Dorsal view, 22 SS, showing *southpaw* (arrowhead). Scale bar equals 40 μm for (A), (C), (D), and (F) and 80 μm for (B), (E), and (G).

(H) Bar graphs showing effect of *ipk1* loss of function on asymmetric gene expression and organ laterality. Scores were tabulated for % with designated sided expression from each in situ hybridization (A–G). For *bmp4+lefty1*, embryos were scored as positive when both *lefty1* in the diencephelon and *bmp4* in the LPM were detected on the same side. No embryos with both *lefty1* and *bmp4* expressed bilaterally were found. n, number of embryos.

signal from intracellular stores (Lemtiri-Chlieh et al., 2003). Thus, we speculated that the LR asymmetry defects in *ipk1*^{MO}-injected embryos may reflect a requirement for proper IP_6 production and IP levels in Ca^{2+} signaling during the first steps of breaking LR symmetry.

To investigate intracellular Ca^{2+} release, we injected 1-cell stage embryos with mRNA encoding a Ca^{2+} indicator protein. Flash-pericam, a chimeric derivative of circularly permuted green fluorescent protein and calmodulin, exhibits increased fluorescence emission with increasing cytosolic Ca^{2+} levels (Nagai et al., 2001).

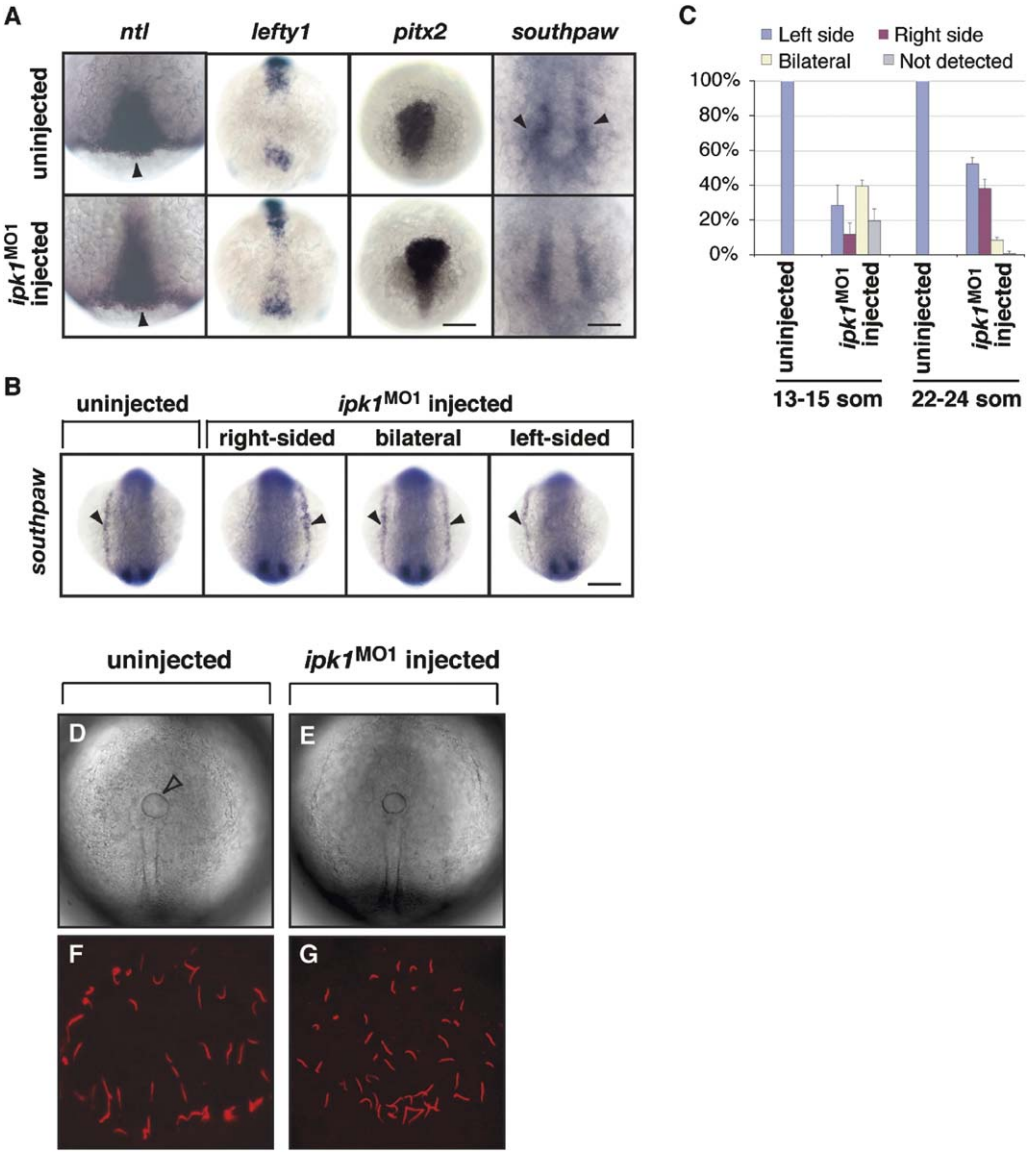

Figure 5. *ipk1* Knockdown Disrupts Early Molecular Asymmetry

(A) Whole-mount in situ hybridizations are shown for uninjected (top) and *ipk1*^{MO1} (bottom) embryos. From left to right: Dorsal views of 85% epibody stage embryos showing *ntl* expression in midline precursor cells, margin cells, and DFCs (first column) (arrowhead points to DFCs); *lefty1* in midline precursor and margin cells (second column); *pitx2* in prechordal plate cells (third column); and dorsal views of the tailbud at 4–6 SS showing bilateral *southpaw* (arrowhead) (fourth column). Scale bar equals 40 μm for first and fourth columns and 80 μm for second and third columns.

(B) *ipk1* knockdown perturbs early asymmetric expression of *southpaw*. Dorsal view, 13–15 SS whole-mount in situ hybridization showing *southpaw* expression (arrowhead) in the left LPM of uninjected embryos (left) and in the right LPM, bilateral, and left LPM of *ipk1*^{MO1} embryos. Scale bar equals 80 μm.

(C) Bar graphs showing scores from three independent experiments for % sided expression of *southpaw* in uninjected and *ipk1*^{MO1} embryos during 13–15 SS and 22–24 SS, each stage collected from the same clutch of embryos. Error bars represent SDs (n = 3).

(D and E) KV morphogenesis is normal in *ipk1*^{MO1} embryos. Ventral view, anterior to the top, DIC images showing KV (arrowhead) of uninjected (D) and *ipk1*^{MO1} (E) 6–8 SS embryos.

(F and G) Cilia in the cells within KV develop normally in *ipk1*^{MO1} embryos. Laser scanning confocal images of cilia (red) detected by fluorescent antiacetylated tubulin immunohistochemistry. Overlay of nine Z sections of 4 μm thickness spanning 36 μm from the floor to the top of KV are shown.

In situ hybridization of injected embryos at 4–6 SS (11.5 hpf) confirmed uniform distribution of flash-pericam mRNA (Supplemental Figure S5). To analyze Ca^{2+} levels, total fluorescence intensity was measured in a defined cellular area surrounding KV at 5–8 SS (example square in Figure 6A). Statistical analysis of mean fluorescence intensities from a population of embryos was conducted to account for slight inherent embryo-to-embryo differences in mounting, imaging focal planes, and flash-pericam mRNA levels. The statistical analysis is summa-

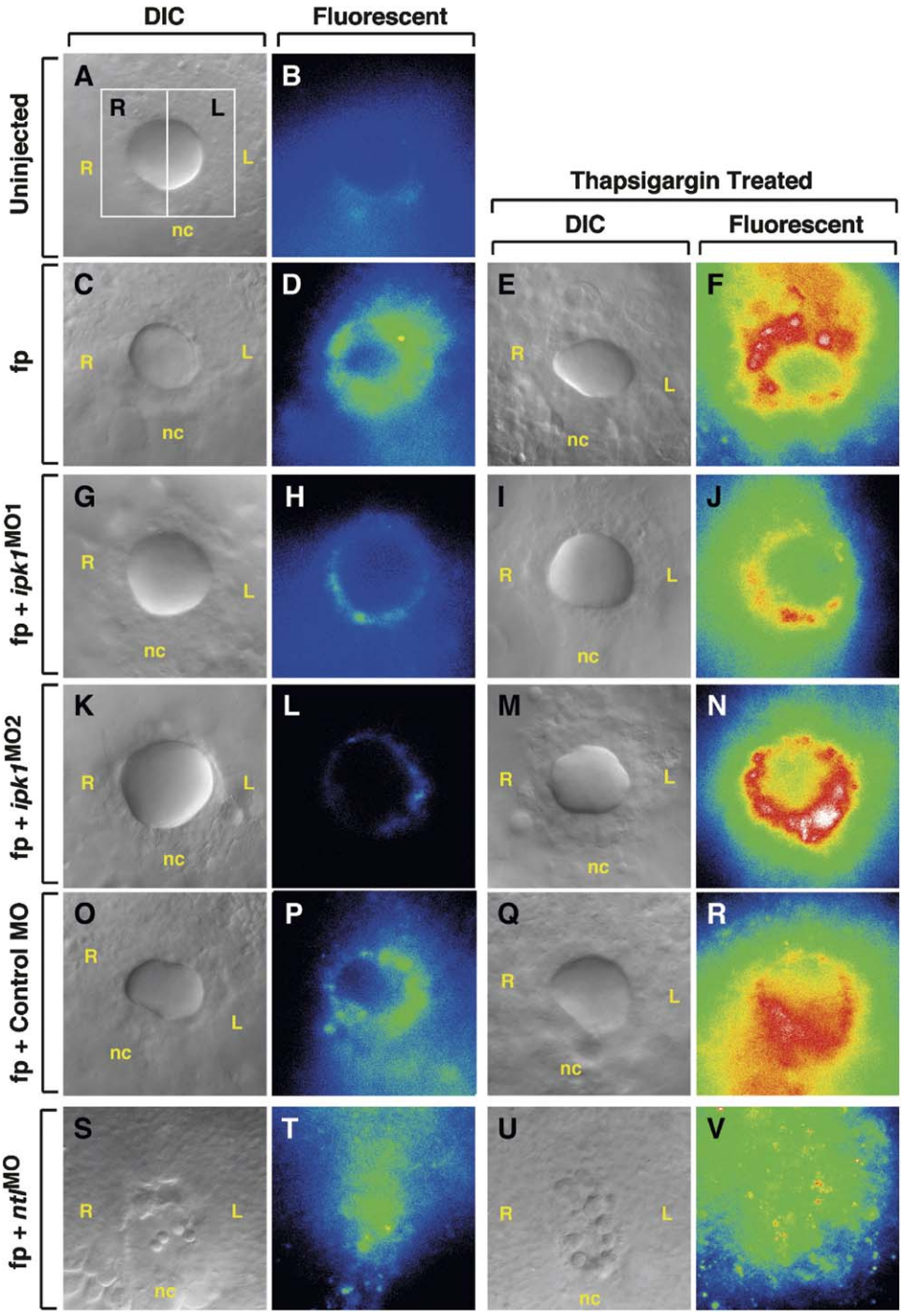

Figure 6. Ca^{2+} Signaling at KV during Early Somite Stages Requires *ipk1*

Representative embryos for each trial are shown with the summary of the statistical analysis from a population of embryos shown in Figure 7A. Embryos were injected at the 1 cell stage with mRNA encoding flash-pericam (fp) and the designated MO. Some embryos were also treated with thapsigargin (right columns). Ca^{2+} patterns at 5–8 SS were imaged by epi-fluorescence microscopy, and images were converted to an intensity scale (red indicating high intensity; yellow/green, moderate; blue/black, low).

(A and B) Autofluorescence of an uninjected 5–8 SS embryo (B) with corresponding DIC (A).

(C and D) A representative embryo injected with only flash-pericam and showing fluorescence at KV (D).

(E and F) Embryos injected with flash-pericam mRNA and treated at 3–4 SS with 3 μM thapsigargin for 90 min.

(G–R) Embryos coinjected with flash-pericam mRNA and either *ipk1*^{MO1} (G–J), *ipk1*^{MO2} (K–N), or *ipk1* control MO (O–R). Embryos coinjected with flash-pericam mRNA and MO were also imaged after thapsigargin treatment (J, N, R). DIC images are shown in (I), (M), and (Q).

(S–V) Embryos coinjected with flash-pericam mRNA and *ntl*^{MO} without (S and T) or with (U and V) thapsigargin treatment. L, left; R, right; nc, notochord.

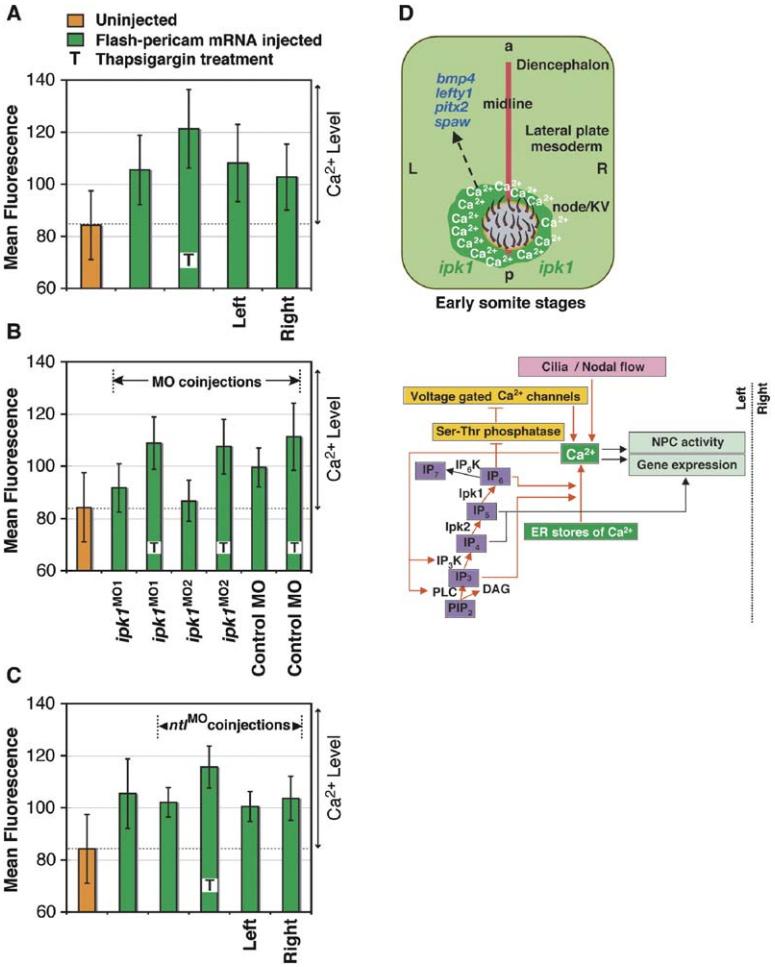

Figure 7. Connections between *ipk1* Function and Ca^{2+} Signaling during Establishment of LR Asymmetry in Zebrafish

(A–C) Panels showing quantitative analysis of Ca^{2+} flux at KV in a population of embryos treated as in Figure 6.

(A) Wild-type embryos have a left-sided Ca^{2+} at KV.

(B) *ipk1* knockdown perturbs Ca^{2+} signaling at KV.

(C) Ca^{2+} flux is symmetric in *ntl*^{MO} embryos that lack of KV morphogenesis. For each panel, mean fluorescent intensities (gray pixel level) for Ca^{2+} levels in KV region were quantified with mean total for the area, mean left, and mean right plotted. Autofluorescence threshold (orange bar) is ~85. Trials for flash-pericam mRNA injections (alone or coinjected with MOs) are shown (green bars). Statistical outcomes of comparisons between different trial populations are in Supplemental Table S3. Student's t test was performed on the measured values, and error bars represent SDs (n). T, thapsigargin.

(D) Model for *ipk1* and IP-mediated propagation of an initial Ca^{2+} flux on the left side of the embryo at KV. Top: *ipk1* is symmetrically expressed in cells enveloping KV and may mediate expansion of asymmetric Ca^{2+} flux initiated by motile cilia. This may drive LR gene expression across cell fields, with the early asymmetric expression of *southpaw* (*spaw*) perturbed when the IP pathway is blocked. Bottom: Extracellular Ca^{2+} influx from cilia function triggers PLC activation for hydrolysis of PIP_2 to produce DAG and soluble IP_3. IP_3 allows generation of inositol polyphosphates by a kinase pathway. IPs may play roles in gene expression (IP_4, IP_5) and/or establishing a self-propagating amplification loop for the Ca^{2+} flux (IP_3, IP_6).

rized in Figure 7A and Supplemental Table S3. Figure 6 shows representative embryos from each trial. Compared to autofluorescence levels in uninjected embryos (Figures 6B and 7A), we observed significant fluorescence in flash-pericam-injected embryos (Figures 6D and 7A). The embryos showed very transient fluorescence, between 5 and 8 SS, with none detected after 10 SS. Notably, this stage corresponds to the time at which KV is thought to initiate LR asymmetry (Essner et al., 2005). We next analyzed flash-pericam-injected embryos for the mean fluorescence intensities from equivalent left and right areas on either side of the midline axis drawn through KV. For the population (n = 27), the left-sided fluorescence intensity showed a statistically significant elevated signal compared to the right side (Figure 7A; Supplemental Table S3). When examining the distribution of sided higher fluorescence in individual embryos, 78% were left-sided, 7% were right-sided, and 15% were symmetric. The small percentage of embryos with symmetric Ca^{2+} signal, or no detectable fluorescence, may have been imaged slightly outside 5–8 SS.

As a control to indicate the capacity for high-level Ca^{2+} signaling, flash-pericam-injected embryos were treated with thapsigargin. Thapsigargin elevates cytosolic free Ca^{2+} concentration, significantly elevating overall Ca^{2+}-based fluorescence in zebrafish embryos (Creton, 2004; Jackson et al., 1988). Thapisgargin treatment elevated fluorescence in KV region, indicating that flash-pericam was a sensitive reporter of Ca^{2+} in zebrafish and, moreover, that the cells in this region had the capacity for Ca^{2+} flux (Figures 6F and 7A). We also examined the distribution of fluorescence in the thapsigargin-treated embryos and found no statistically significant difference in the total population between the levels on the left and right sides of the axis through KV. Thus, flash-pericam fluorescence reveals a transient, left-biased flux of intracellular Ca^{2+} near KV in normal zebrafish embryogenesis.

ipk1 Knockdown Perturbs Ca^{2+} Signaling at KV

To investigate whether *ipk1* function is required for Ca^{2+} flux at KV, embryos were coinjected with flash-pericam mRNA and either *ipk1*^{MO1} or *ipk1*^{MO2}. Fluorescence levels were measured at 5–8 SS, in the presence and absence of thapsigargin. In KV region of *ipk1*^{MO}-injected embryos, fluorescence was reduced to levels that were statistically equivalent to autofluorescence background levels (Figures 6H, 6L, and 7B; Supplemental Table S3). There was also no difference between fluorescence levels on the left and right sides of the axis through KV. However, the dramatic elevation of fluorescence caused

by thapsigargin treatment indicated that the embryos were capable of intracellular Ca^{2+} release (Figures 6J, 6N, and 7B). Thus, loss of *ipk1* function inhibited intracellular Ca^{2+} flux in cells surrounding KV, raising the possibility that *ipk1* influences LR asymmetry by mediating changes in intracellular Ca^{2+} concentrations.

Asymmetric Ca^{2+} Flux Is Linked to KV Morphogenesis

To test whether the Ca^{2+} flux was dependent on the presence of KV, we coinjected embryos with *ntl*^{MO} (Nasevicius and Ekker, 2000) and flash-pericam mRNA. KV morphogenesis requires *ntl* function (Figure 6S; Amack and Yost, 2004; Melby et al., 1996). At 5–8 SS, fluorescence was measured in the ventral tailbud region where KV would normally form (Figures 6T and 7C). The total mean fluorescence level was not statistically different from embryos injected with only flash-pericam (Figure 7C; Supplemental Table S3). Thapsigargin treatment also increased the fluorescence levels in flash-pericam *ntl*^{MO}-injected embryos (Figures 6V and 7C; Supplemental Table S3). Thus, the ability to undergo a transient Ca^{2+} flux in this region does not depend upon KV morphogenesis. Next, we analyzed *ntl*^{MO}-injected embryos for the distribution of Ca^{2+} signal on either side of the axis relative to notochord. When compared in a Student's t test, the p value of 0.3924 indicated that the levels were not different on the left and right sides (Figure 7C; Supplemental Table S3). Loss of asymmetric Ca^{2+} flux was not due to disruption of *ipk1* expression, as in situ hybridization showed that *ntl*^{MO} embryos expressed *ipk1* normally (Supplemental Figure S4). Thus, our data indicate that left-biased intracellular Ca^{2+} flux requires both an intact KV and *ipk1* function.

Discussion

Here we provide evidence that highly phosphorylated inositols are required in a critical aspect of axial specification during early embryonic patterning. Specifically, we discovered that *ipk1* plays a role in establishing LR asymmetry in zebrafish presumably through its function as an IP_5 2-kinase. Loss of *ipk1* function resulted in a concordant randomization of both molecular and morphological asymmetries in embryos and eliminated left-biased Ca^{2+} flux at KV, an organ implicated in early steps of LR patterning. Thus, IP metabolism regulates intracellular Ca^{2+} flux in zebrafish embryos, and IPs and intracellular Ca^{2+} flux are key linked components of the signaling mechanism that mediates early events in LR morphogenesis.

Multiple soluble IPs may influence the establishment of LR asymmetry and Ca^{2+} flux. Based on our analysis of IP levels in *ipk1*^{MO1} embryos, the defects could result from lowered IP_6 production, the coincident inherent loss of IP_7, or increased accumulation of the upstream IP_4 and IP_5. Interestingly, we found that IP_3 is the most predominant soluble IP in labeled zebrafish embryos. This is not true in yeast, flies, or cultured vertebrate cell lines where IP_5 or IP_6 is the major steady-state IP (Seeds et al., 2004; Verbsky et al., 2005; York et al., 1999). Elevated IP_3 levels have also been reported during early embryogenesis in frogs, and expression of the IP_3 receptor is elevated during early embryonic development (Kume, 1999). Taken together, we have established that regulated IP production by the IP signaling machinery plays an essential role in early vertebrate development.

Model for IP Role in Establishing LR Asymmetry

Our observation that loss of *ipk1* function randomizes LR asymmetry is strikingly similar to the phenotype of mice with mutations of *iv*, which encodes left-right dynein (Supp et al., 1997). Zebrafish KV cells express *left-right dynein-related1 (lrdr1)* and form motile cilia, and *lrdr1* function is necessary in KV cells to establish LR asymmetry (Essner et al., 2005). As shown in Figure 7D, we propose that regulation of intracellular Ca^{2+} levels by IP signaling is a obligate step in transducing the LR specification signal initiated by ciliary action at KV to paraxial mesoderm. This model would result in left-biased patterns of gene expression and is based on the following key observations. First, cells surrounding KV express *ipk1*. Second, in wild-type embryos, a transient flux of intracellular Ca^{2+} at KV is consistently greater in cells on the left side than in those on the right side. This Ca^{2+} flux is dependent on *ipk1* function. Third, a concordant randomization of both molecular and anatomical asymmetries is observed in embryos with reduced Ipk1 function. However, KV and cilia morphogenesis are not affected. Finally, the lack of left-sided Ca^{2+} flux in *ntl*^{MO} embryos suggests that cilia organization is critical for proper spatial activation of the Ca^{2+} signal.

We speculate that once an initial extracellular Ca^{2+} influx on the left side of the embryo is triggered by ciliary function during KV morphogenesis, an IP-based propagation of a left-sided intracellular Ca^{2+} flux results. A key step in the model involves the initial extracellular Ca^{2+} influx activating PLC and IP_3-kinase activities (Berridge et al., 2000), resulting ultimately in IP_6 production by Ipk1. IPs are excellent candidates for low-molecular-weight determinants that could move through gap junctions to influence multicellular fields in the embryo (Levin and Mercola, 1998; Mercola, 2003; Webb and Miller, 2003). Future work will also need to address whether IPs affect cilia function directly. We favor the model shown in Figure 7D, given the strong prior documentation of IPs regulating intracellular Ca^{2+} fluxes directly. Well-characterized IP_3 receptors mediate release of intracellular endomembrane Ca^{2+} stores (Berridge et al., 2000). IP_6 could also induce Ca^{2+} release from endomembrane stores (Lemtiri-Chlieh et al., 2003), and IP_4 may influence Ca^{2+} signaling (Hermosura et al., 2000). Inhibition of serine-threonine protein phosphatases by IP_6 may activate the voltage-gated Ca^{2+} channels (Larsson et al., 1997), further amplifying cytosolic Ca^{2+}.

Evidence for Ca^{2+} signaling affecting gene expression is extensive (Berridge et al., 2000). Ca^{2+} can also regulate nuclear pore complex structure and permeability (Perez-Terzic et al., 1996). Alternatively, or coincidently, the IPs themselves could directly influence gene expression independent of the Ca^{2+} flux. IPs may modulate chromatin remodeling, transcription, and nuclear mRNA export (Odom et al., 2000; Shen et al., 2003; Steger et al., 2003; York et al., 1999). The direct targets

for such IP action in regulating Ca^{2+} fluxes are not fully resolved, and the receptors for the most highly phosphorylated inositides are unknown.

A left-biased flux in intracellular Ca^{2+} levels also occurs near the mouse node (McGrath et al., 2003). The Ca^{2+} flux in mice is associated with the presence of monocilia on the node cells, with two classes of cilia possibly playing roles (McGrath et al., 2003; Tabin and Vogan, 2003). One class, the immotile/sensory cilia, is proposed to detect the movement of extracellular fluid driven by a second class of motile cilia. In this model, deflection of sensory cilia might trigger Ca^{2+}/cation transport through channels containing polycystin-2 (Koulen et al., 2002; McGrath et al., 2003; Nauli et al., 2003). In zebrafish, cilia form within KV, and KV development is necessary for establishing normal LR asymmetries (Amack and Yost, 2004; Cooper and D'Amico, 1996; Essner et al., 2002; Essner et al., 2005). Our findings are consistent with the hypothesis that Ca^{2+} signaling at KV is functionally similar to the mechanism at the mouse node.

We predict that a role for IP production in transducing LR information will be a conserved mechanism in all vertebrates. There are multiple PLC pathways and isoforms in vertebrates (Irvine, 2003); however, all apparently converge on a single Ipk1 (Verbsky et al., 2002). The genes encoding Ipk1 in various organisms result in enzymes with highly conserved putative catalytic site motifs, as reflected in our cross-species complementation studies (Figure 1; Ives et al., 2000; Verbsky et al., 2002). Linking IP levels and production to a fundamental aspect of early vertebrate development sets the precedent for discovering future roles of IPs at other steps in development and organogenesis of multicellular organisms.

Experimental Procedures

Plasmid Constructs and Yeast Strains

Total RNA from zebrafish embryos (4 hpf) was isolated using Trizol (Invitrogen) and treated with RQ1 RNase-free DNase (Promega), and cDNA was prepared using Superscript-II-RT and oligo(dT) primer (Invitrogen). To clone *ipk1*, specific cDNA was amplified by PCR with oligonucleotide primers 1 and 6 (Supplemental Table S1). The PCR product was cloned in the EcoRV site of pBluescript SK (Stratagene), resulting in pSW3007, and in the StuI site of $pCS2^+$ (Turner and Weintraub, 1994) for pSW3015, and then sequenced. The sequence encoding zebrafish Ipk1 was PCR amplified from pSW3007 using the 1-NcoI and 6-SalI primer pair (Supplemental Table S1) and inserted into a yeast expression vector by replacing the NcoI-SalI fragment of pSW747 (Watkins et al., 1998). This pSW3013 places *ipk1* behind the *GLE1* promoter and encodes a fusion of full-length zebrafish Ipk1 and the first six amino acids of Gle1. The XhoI-BamHI fragment of pSW3015 was cloned in pVT101T, placing zebrafish *ipk1* under control of *ADH* promoter to give pSW3016. The BamH1-XhoI fragment of pSW3007 was cloned in pcDNA3 (Invitrogen) for *ipk1* under control of T7 promoter in pSW3011. Genotypes of *S. cerevisiae* strains are in Supplemental Table S2.

Embryos

Embryos were collected from single pair matings and raised at 28.5°C in embryo medium (EM) (15 mM NaCl, 0.5 mM KCl, 1 mM $CaCl_2$, 1 mM $MgSO_4$, 0.15 mM KH_2PO_4, 0.05 mM NH_2PO_4, 0.7 mM $NaHCO_3$) and staged according to hpf and morphological criteria (Kimmel et al., 1995).

Analysis of Cellular ^{3}H-Inositol-Labeled IP Levels

The soluble IP profiles of yeast cell lysates were determined as described (York et al., 1999). For IP profiles of zebrafish embryos, embryos were injected with ^{3}H-inositol (500 pCi) at 1–16 cell stage either with or without $ipk1^{MO1}$ (7.5 ng). Embryos were grown until 4–6 SS (11.5 hpf) and dechorionated with pronase (0.5 mg/ml). Soluble IPs were extracted by adding 372 μl chloroform/methanol (1:2, v/v) and 100 μl of glass beads to 250 dechorionated embryos. Samples were analyzed by HPLC (Whatman partisphere SAX strong-anion exchange column, 4.6 × 125 mm) in an identical manner as yeast cell samples.

ipk1 Knockdown Strategies

Morpholino antisense oligonucleotides (MO) were purchased from Gene Tools, LLC. The $ipk1^{MO1}$ (5′-GTCCATTTTATCCAGTTCCATA ACC-3′) was complementary to sequence spanning the translation start codon, whereas the control MO had five mismatches as underlined (5′-GTGCAATTTATGCACTTGCATAACC-3′). The $ipk1^{gripNA}$ (5′-CATTTTATCCAGTTCCAT-3′), an antisense peptide nucleic acid, was obtained from Active Motif. $ipk1^{MO2}$ (5′-ATACAGTCATTTAC* CAGGTCGTTCT-3′) anneals to the exon4-intron4 junction (asterisk indicates position of splice site in complementary sequence). MO and GripNA were dissolved in water, dilutions of 2.5–7.5 μg/μl were made in 1× Danieau solution (58 mM NaCl, 0.7 mM KCl, 0.4 mM $MgSO_4$, 0.6 mM $Ca(NO_3)_2$, 5 mM HEPES [pH 7.6]), and 1–2 nl was injected at the 1–2 cell stage into the yolk, just under the blastoderm.

In Situ Hybridization

In situ hybridizations were performed as described (Hauptmann and Gerster, 2000). *ipk1* antisense RNA probe was prepared from EcoRI linearized pSW3007 using T7 RNA polymerase. Previously described probes include those for *bmp4* (Chen et al., 1997), *gata6* (Reiter et al., 1999), *foxA3* (Field et al., 2003), *lefty1* (Thisse and Thisse, 1999), *pitx2* (Essner et al., 2000), *southpaw* (Long et al., 2003), *ntl* (Schulte-Merker et al., 1994), *netrin1b* (Strahle et al., 1997), and *col2a1* (Yan et al., 1995). For two-probe detection, we used digoxygenin-labeled *ipk1* and fluorescein-labeled *ntl.* Embryos were embedded in 1.5% agarose/30% sucrose and frozen in 2-methyl-butane chilled by immersion in liquid nitrogen. Sections (10 μm) were obtained using a cryostat microtome. Images were obtained using a Retiga Exi cooled CCD camera (Qimaging) mounted on a compound microscope and OPENLAB software and imported into Adobe Photoshop, and manipulation was limited to levels, curves, hue, and saturation adjustments.

Immunohistochemistry

Embryos were fixed overnight at 4°C in 4% paraformaldehyde, 0.15 mM $CaCl_2$, 4% sucrose in 0.1 M phosphate buffer (pH 7.3). Indirect immunofluorescence was performed using 1:100 mouse anti-acetylated tubulin monoclonal antibody (Sigma) and 1:200 Alexa Fluor 568 goat anti-mouse conjugate (Molecular Probes). Embryos were mounted in methyl cellulose (3%) on bridged slides, and images were obtained using a Zeiss LSM510 Meta laser scanning confocal microscope.

Ca^{2+} Imaging

mRNA encoding flash-pericam (Nagai et al., 2001) was synthesized from a linearized flash-pericam/pcDNA3 clone (generously provided by David Piston) using T7 RNA polymerase and mMassage mMachine kit (Ambion) and purified with a Sephadex G50 (fine) Spin Column (Roche). Titered amounts of flash-pericam mRNA were injected at 1-cell stage, and 50 pg was used for all subsequent experiments as these embryos grew normally. Ca^{2+} patterns within KV and in cells enveloping it were imaged by epi-fluorescence microscopy. Embryos were dechorionated, mounted in SeaPlaque low-melting agarose (Biowhittaker Molecular Applications) (1.2% in EM) in microwells of Glass Bottom Culture Dishes (MatTek), and covered with EM. After 15 min, images were acquired using OPENLAB software (Improvision) on a Zeiss Axiovert 200 inverted fluorescent microscope equipped with a Retiga Exi Fast camera (Qimaging). 2 mM thapsigargin (LC Laboratories) in DMSO was diluted in EM. Embryos were dechorionated at the beginning

of KV morphogenesis (3–4 SS), treated with 2.5 ml of 3 μM thapsigargin for 90 min at 28.5°C in a 35 × 10 mm tissue culture dish layered with 1.2 ml of 1.5% agarose, and then imaged for fluorescence. For flash-pericam mRNA and MO coinjection experiments, 50 pg mRNA was injected with either 7.5 ng (*ipk1*^{MO1}/*ipk1*^{MO2}/Control MO) or 4 ng (*ntl*^{MO}) MO.

Fluorescent images of Ca^{2+} signals were analyzed using Volocity software (Improvision). Fluorescent intensities (gray pixel level) were measured in a square area surrounding KV that was subdivided into two equal halves with respect to the LR axis (Figure 6A). Mean gray pixel values were obtained for each half (R versus L). Total average, left-sided average, and right-sided average mean gray pixel values were determined in a population of embryos. Statistical analysis using the Student's t test of the measured values was performed using Quickcalcs program (GraphPad) (Supplemental Table S3).

Supplemental Data

Supplemental Data include five figures and three tables and can be found with this article online at http://www.developmentalcell.com/cgi/content/full/9/1/133/DC1/.

Acknowledgments

We are indebted to Christopher V.E. Wright for critical input and guidance throughout the project and to David Piston for advice on Ca^{2+} imaging. We thank Katherine Lewis and Judith Eisen for the *ntl*^{MO} gift and Joshua Gamse and Appel and Wente laboratory members for discussions. Confocal microscopy was performed using equipment made available by the VUMC Cell Imaging Core Resource, supported by NIH grants 1S10RR15682, CA68485, and DK20593. This work was supported by grants from the National Institutes of Health (HD38118 to B.A., GM51912 to S.R.W.), a Kirsch Investigator Award from the Steven and Michelle Kirsch Foundation (to S.R.W.), the Vanderbilt University Academic Venture Capital Fund, and a VU Zebrafish Pilot Project Grant.

Received: November 7, 2004
Revised: March 30, 2005
Accepted: May 3, 2005
Published: July 5, 2005

References

Amack, J.D., and Yost, H.J. (2004). The T box transcription factor no tail in ciliated cells controls zebrafish left-right asymmetry. Curr. Biol. *14*, 685–690.

Berridge, M.J., Lipp, P., and Bootman, M.D. (2000). The versatility and universality of calcium signalling. Nat. Rev. Mol. Cell Biol. *1*, 11–21.

Bisgrove, B.W., Essner, J.J., and Yost, H.J. (2000). Multiple pathways in the midline regulate concordant brain, heart and gut left-right asymmetry. Development *127*, 3567–3579.

Capdevila, J., Vogan, K.J., Tabin, C.J., and Izpisua Belmonte, J.C. (2000). Mechanisms of left-right determination in vertebrates. Cell *101*, 9–21.

Chen, J.N., van Eeden, F.J., Warren, K.S., Chin, A., Nusslein-Volhard, C., Haffter, P., and Fishman, M.C. (1997). Left-right pattern of cardiac BMP4 may drive asymmetry of the heart in zebrafish. Development *124*, 4373–4382.

Cooper, M.S., and D'Amico, L.A. (1996). A cluster of noninvoluting endocytic cells at the margin of the zebrafish blastoderm marks the site of embryonic shield formation. Dev. Biol. *180*, 184–198.

Creton, R. (2004). The calcium pump of the endoplasmic reticulum plays a role in midline signaling during early zebrafish development. Brain Res. Dev. Brain Res. *151*, 33–41.

Essner, J.J., Branford, W.W., Zhang, J., and Yost, H.J. (2000). Mesendoderm and left-right brain, heart and gut development are differentially regulated by pitx2 isoforms. Development *127*, 1081–1093.

Essner, J.J., Vogan, K.J., Wagner, M.K., Tabin, C.J., Yost, H.J., and Brueckner, M. (2002). Conserved function for embryonic nodal cilia. Nature *418*, 37–38.

Essner, J.J., Amack, J.D., Nyholm, M.K., Harris, E.B., and Yost, H.J. (2005). Kupffer's vesicle is a ciliated organ of asymmetry in the zebrafish embryo that initiates left-right development of the brain, heart and gut. Development *132*, 1247–1260.

Field, H.A., Ober, E.A., Roeser, T., and Stainier, D.Y. (2003). Formation of the digestive system in zebrafish. I. Liver morphogenesis. Dev. Biol. *253*, 279–290.

Hamada, H., Meno, C., Watanabe, D., and Saijoh, Y. (2002). Establishment of vertebrate left-right asymmetry. Nat. Rev. Genet. *3*, 103–113.

Hauptmann, G., and Gerster, T. (2000). Multicolor whole-mount in situ hybridization. Methods Mol. Biol. *137*, 139–148.

Hermosura, M.C., Takeuchi, H., Fleig, A., Riley, A.M., Potter, B.V.L., Hirata, M., and Penner, R. (2000). $InsP_4$ facilitates store-operated calcium influx by inhibition of $InsP_3$ 5-phosphatase. Nature *408*, 735–740.

Irvine, R.F. (2003). 20 years of Ins(1,4,5)P3, and 40 years before. Nat. Rev. Mol. Cell Biol. *4*, 586–590.

Irvine, R.F., and Schell, M.J. (2001). Back in the water: the return of the inositol phosphates. Nat. Rev. Mol. Cell Biol. *2*, 327–338.

Ives, E.B., Nichols, J., Wente, S.R., and York, J.D. (2000). Biochemical and functional characterization of inositol 1,3,4,5, 6-pentakisphosphate 2-kinases. J. Biol. Chem. *275*, 36575–36583.

Jackson, T.R., Patterson, S.I., Thastrup, O., and Hanley, M.R. (1988). A novel tumour promoter, thapsigargin, transiently increases cytoplasmic free Ca^{2+} without generation of inositol phosphates in NG115–401L neuronal cells. Biochem. J. *253*, 81–86.

Kimmel, C.B., Ballard, W.W., Kimmel, S.R., Ullmann, B., and Schilling, T.F. (1995). Stages of embryonic development of the zebrafish. Dev. Dyn. *203*, 253–310.

Koulen, P., Cai, Y., Geng, L., Maeda, Y., Nishimura, S., Witzgall, R., Ehrlich, B.E., and Somlo, S. (2002). Polycystin-2 is an intracellular calcium release channel. Nat. Cell Biol. *4*, 191–197.

Kramer, K.L., Barnette, J.E., and Yost, H.J. (2002). PKCgamma regulates syndecan-2 inside-out signaling during *Xenopus* left-right development. Cell *111*, 981–990.

Kume, S. (1999). Role of the inositol 1,4,5-trisphosphate receptor in early embryonic development. Cell. Mol. Life Sci. *56*, 296–304.

Larsson, O., Barker, C.J., Sj-oholm, A., Carlqvist, H., Michell, R.H., Bertorello, A., Nilsson, T., Honkanen, R.E., Mayr, G.W., Zwiller, J., and Berggren, P.O. (1997). Inhibition of phosphatases and increased Ca^{2+} channel activity by inositol hexakisphosphate. Science *278*, 471–474.

Lemtiri-Chlieh, F., MacRobbie, E.A., Webb, A.A., Manison, N.F., Brownlee, C., Skepper, J.N., Chen, J., Prestwich, G.D., and Brearley, C.A. (2003). Inositol hexakisphosphate mobilizes an endomembrane store of calcium in guard cells. Proc. Natl. Acad. Sci. USA *100*, 10091–10095.

Levin, M., and Mercola, M. (1998). Gap junctions are involved in the early generation of left-right asymmetry. Dev. Biol. *203*, 90–105.

Levin, M., Thorlin, T., Robinson, K.R., Nogi, T., and Mercola, M. (2002). Asymmetries in H^+/K^+-ATPase and cell membrane potentials comprise a very early step in left-right patterning. Cell *111*, 77–89.

Long, S., Ahmad, N., and Rebagliati, M. (2003). The zebrafish nodal-related gene *southpaw* is required for visceral and diencephalic left-right asymmetry. Development *130*, 2303–2316.

McGrath, J., Somlo, S., Makova, S., Tian, X., and Brueckner, M. (2003). Two populations of node monocilia initiate left-right asymmetry in the mouse. Cell *114*, 61–73.

Melby, A.E., Warga, R.M., and Kimmel, C.B. (1996). Specification of cell fates at the dorsal margin of the zebrafish gastrula. Development *122*, 2225–2237.

Mercola, M. (2003). Left-right asymmetry: nodal points. J. Cell Sci. *116*, 3251–3257.

Nagai, T., Sawano, A., Park, E.S., and Miyawaki, A. (2001). Circularly permuted green fluorescent proteins engineered to sense Ca^{2+}. Proc. Natl. Acad. Sci. USA *98*, 3197–3202.

Nasevicius, A., and Ekker, S.C. (2000). Effective targeted gene 'knockdown' in zebrafish. Nat. Genet. *26*, 216–220.

Nauli, S.M., Alenghat, F.J., Luo, Y., Williams, E., Vassilev, P., Li, X., Elia, A.E., Lu, W., Brown, E.M., Quinn, S.J., et al. (2003). Polycystins 1 and 2 medicate mechanosensation in the primary cilium of kidney cells. Nat. Genet. *33*, 129–137.

Nonaka, S., Tanaka, Y., Okada, Y., Takeda, S., Harada, A., Kanai, Y., Kido, M., and Hirokawa, N. (1998). Randomization of left-right asymmetry due to loss of nodal cilia generating leftward flow of extraembryonic fluid in mice lacking KIF3B motor protein. Cell *95*, 829–837.

Nonaka, S., Shiratori, H., Saijoh, Y., and Hamada, H. (2002). Determination of left-right patterning of the mouse embryo by artificial nodal flow. Nature *418*, 96–99.

Odom, A.R., Stahlberg, A., Wente, S.R., and York, J.D. (2000). A role for nuclear inositol 1,4,5-trisphosphate kinase in transcriptional control. Science *287*, 2026–2029.

Okada, Y., Nonaka, S., Tanaka, Y., Saijoh, Y., Hamada, H., and Hirokawa, N. (1999). Abnormal nodal flow precedes situs inversus in *iv* and *inv* mice. Mol. Cell *4*, 459–468.

Pendaries, C., Tronchere, H., Plantavid, M., and Payrastre, B. (2003). Phosphoinositide signaling disorders in human diseases. FEBS Lett. *546*, 25–31.

Perez-Terzic, C., Pyle, J., Jaconi, M., Stehno-Bittel, L., and Clapham, D.E. (1996). Conformational states of the nuclear pore complex induced by depletion of nuclear Ca^{2+} stores. Science *273*, 1875–1877.

Raya, A., Kawakami, Y., Rodriguez-Esteban, C., Ibanes, M., Rasskin-Gutman, D., Rodriguez-Leon, J., Buscher, D., Feijo, J.A., and Izpisua Belmonte, J.C. (2004). Notch activity acts as a sensor for extracellular calcium during vertebrate left-right determination. Nature *427*, 121–128.

Rebagliati, M., Toyama, R., Haffter, P., and Dawid, I.B. (1998). *cyclops* encodes a nodal-related factor involved in midline signaling. Proc. Natl. Acad. Sci. USA *95*, 9932–9937.

Reiter, J.F., Alexander, J., Rodaway, A., Yelon, D., Patient, R., Holder, N., and Stainier, D.Y. (1999). Gata5 is required for the development of the heart and endoderm in zebrafish. Genes Dev. *13*, 2983–2995.

Sampath, K., Rubinstein, A.L., Cheng, A.M., Liang, J.O., Fekany, K., Solnica-Krezel, L., Korzh, V., Halpern, M.E., and Wright, C.V. (1998). Induction of zebrafish ventral brain and floorplate requires *cyclops/nodal* signalling. Nature *395*, 185–189.

Schulte-Merker, S., van Eeden, F.J., Halpern, M.E., Kimmel, C.B., and Nusslein-Volhard, C. (1994). *no tail* (*ntl*) is the zebrafish homologue of the mouse T (Brachyury) gene. Development *120*, 1009–1015.

Seeds, A.M., Sandquist, J.C., Spana, E.P., and York, J.D. (2004). A molecular basis for inositol polyphosphate synthesis in *Drosophila melanogaster*. J. Biol. Chem. *279*, 47222–47232.

Shears, S.B. (2004). How versatile are inositol phosphate kinases? Biochem. J. *377*, 265–280.

Shen, X., Xiao, H., Ranallo, R., Wu, W.H., and Wu, C. (2003). Modulation of ATP-dependent chromatin-remodeling complexes by inositol polyphosphates. Science *299*, 112–114.

Steger, D.J., Haswell, E.S., Miller, A.L., Wente, S.R., and O'Shea, E.K. (2003). Regulation of chromatin remodeling by inositol polyphosphates. Science *299*, 114–116.

Strahle, U., Fischer, N., and Blader, P. (1997). Expression and regulation of a netrin homologue in the zebrafish embryo. Mech. Dev. *62*, 147–160.

Supp, D.M., Witte, D.P., Potter, S.S., and Brueckner, M. (1997). Mutation of an axonemal dynein affects left-right asymmetry in inversus viscerum mice. Nature *389*, 963–966.

Tabin, C.J., and Vogan, K.J. (2003). A two-cilia model for vertebrate left-right axis specification. Genes Dev. *17*, 1–6.

Thisse, C., and Thisse, B. (1999). Antivin, a novel and divergent member of the TGFbeta superfamily, negatively regulates mesoderm induction. Development *126*, 229–240.

Thompson, J.D., Higgins, D.G., and Gibson, T.J. (1994). CLUSTAL W: improving the sensitivity of progressive multiple sequence alignment through sequence weighting, position-specific gap penalties and weight matrix choice. Nucleic Acids Res. *22*, 4673–4680.

Turner, D.L., and Weintraub, H. (1994). Expression of achaete-scute homolog 3 in *Xenopus* embryos converts ectodermal cells to a neural fate. Genes Dev. *8*, 1434–1447.

Verbsky, J.W., Wilson, M.P., Kisseleva, M.V., Majerus, P.W., and Wente, S.R. (2002). The synthesis of inositol hexakisphosphate. Characterization of human inositol 1,3,4,5,6-pentakisphosphate 2-kinase. J. Biol. Chem. *277*, 31857–31862.

Verbsky, J.W., Chang, S.-C., Wilson, M.P., Mochizuki, Y., and Majerus, P.W. (2005). The pathway for the production of inositol hexakisphosphate in human cells. J. Biol. Chem. *280*, 1911–1920.

Watkins, J.L., Murphy, R., Emtage, J.L., and Wente, S.R. (1998). The human homologue of *Saccharomyces cerevisiae Gle1p* is required for poly(A)+ RNA export. Proc. Natl. Acad. Sci. USA *95*, 6779–6784.

Webb, S.E., and Miller, A.L. (2003). Calcium signalling during embryonic development. Nat. Rev. Mol. Cell Biol. *4*, 539–551.

Wright, C.V. (2001). Mechanisms of left-right asymmetry: what's right and what's left? Dev. Cell *1*, 179–186.

Yan, Y.L., Hatta, K., Riggleman, B., and Postlethwait, J.H. (1995). Expression of a type II collagen gene in the zebrafish embryonic axis. Dev. Dyn. *203*, 363–376.

Yang, S.N., Yu, J., Mayr, G.W., Hofmann, F., Larsson, O., and Berggren, P.O. (2001). Inositol hexakisphosphate increases L-type Ca^{2+} channel activity by stimulation of adenylyl cyclase. FASEB J. *15*, 1753–1763.

York, J.D., Odom, A.R., Murphy, R., Ives, E.B., and Wente, S.R. (1999). A Phospholipase C-dependent inositol polyphosphate kinase pathway required for efficient messenger RNA export. Science *285*, 96–100.